

VAPOR: Legged Robot Navigation in Outdoor Vegetation using Offline Reinforcement Learning

Kasun Weerakoon¹, Adarsh Jagan Sathyamoorthy¹, Mohamed Elnoor¹, and Dinesh Manocha²

Abstract—We present VAPOR, a novel method for autonomous legged robot navigation in unstructured, densely vegetated outdoor environments using Offline Reinforcement Learning (RL). Our method trains a novel RL policy from unlabeled data collected in real outdoor vegetation. This policy uses height and intensity-based cost maps derived from 3D LiDAR point clouds, a goal cost map, and processed proprioception data as state inputs, and learns the physical and geometric properties of the surrounding vegetation such as height, density, and solidity/stiffness for navigation. Instead of using end-to-end policy actions, the fully-trained RL policy’s Q network is used to evaluate dynamically feasible robot actions generated from a novel adaptive planner capable of navigating through dense narrow passages and preventing entrapment in vegetation such as tall grass and bushes. We demonstrate our method’s capabilities on a legged robot in complex outdoor vegetation. We observe an improvement in success rates, a decrease in average power consumption, and decrease in normalized trajectory length compared to both existing end-to-end offline RL and outdoor navigation methods.

I. INTRODUCTION

Autonomous robot navigation in outdoor environments is an essential capability for many applications, including precision agriculture [1], search and rescue operations in forested environments [2], reconnaissance[3], etc. There are two major challenges in navigating in these densely vegetated scenarios. Firstly, the robot must perceive and differentiate non-solid/pliable obstacles (e.g. tall grass), from solid/non-pliable obstacles (e.g. trees) [4]. Pliable obstacles can be safely traversed through, whereas non-pliable obstacles must be avoided. Secondly, apart from avoiding collisions, the robot also faces challenges such as narrow passages (where the available free space is lower than the robot’s smallest dimension), and scenarios where the vegetation could wrap/attach onto the robot and entrap it. The robot’s navigation must be capable of handling such adverse situations.

To address perception challenges in dense vegetation, existing methods have used RGB image inputs [4], [5], [6], to identify pliable vegetation such as tall grass and used this information for navigation. However, RGB images suffer from a low field of view (FOV), are susceptible to changes in the ambient lighting, and struggle to differentiate visually similar vegetation with different traversability properties. Lidar point clouds [7], [8] detect the shapes and dimensions of solid obstacles accurately but suffer from scattering in the



Fig. 1: Navigation scenario in complex outdoor vegetation where the robot could lead to entrapment.

presence of thin obstacles such as tall grass. This leads to fewer points being reflected to the lidar, causing inaccurate representations of thin, pliable obstacles. However, recent research suggests that the intensity of such reflected points could be used to assess an object’s density and hence its pliability which are inversely related. Therefore, lidar points (indicated by their x, y, z location, and intensity) reflected from objects can be used to first assess its pliability and then its dimensions, if it is solid.

To deal with the navigational challenges in dense vegetation, existing methods have employed traversability cost maps [4] along with a model-based motion planner [9], or used end-to-end reinforcement learning (RL)-based planners [5], etc. However, such strategies have a few limitations. For instance, model-based planners require non-trivial hand-crafted objectives that sometimes require extensive domain knowledge to exhibit the desired behaviors. Conversely, end-to-end RL-based planners have reward functions that are typically easier to design since they deal only with rewarding and penalizing desirable and undesirable behaviors respectively. However, RL-based planners suffer from sim-to-real transfer issues [10] in which a planner’s performance degrades significantly when transferred to real-world environments from simulations. Additionally, end-to-end models could produce dynamically infeasible velocities for the robot resulting in oscillatory and jerky motions.

Main contributions: To address these shortcomings, we propose VAPOR, an offline RL-based trajectory evaluation model combined with a holonomic planner designed to generate dynamically feasible velocities to operate a legged robot in dense vegetation. VAPOR’s offline RL formulation

¹ Authors are with Dept. of Electrical and Computer Engineering, University of Maryland, College Park, MD, USA. kasunw@umd.edu, asathyam@umd.edu, melnoor@umd.edu

² Author is with Dept. of Computer Science, University of Maryland, College Park, MD, USA. upatel22@umd.edu, dm@cs.umd.edu

allows it to be trained using data collected in the real world and annotated minimally [11], alleviating sim-to-real transfer issues. The novel components of our work are:

- We propose a novel observation space to sense dense vegetation consisting of robot-centric height and intensity grid maps obtained by processing lidar point clouds, and a goal map indicating the distance and direction to the robot's goal. The height and intensity maps accurately represent the height and solidity or inversely, the pliability of the surrounding vegetation, while the goal map aids with spatially correlating them with the robot's intended motion direction during training.
- We propose a novel offline reinforcement learning-based Q-network to evaluate the robot's candidate actions/velocities in terms of their ability to reach the goal, avoid solid, non-pliable vegetation and other desirable behaviors. The network consists of spatial and channel attention layers to learn the spatial correlations between the maps in the observation space and is trained using real-world data collected in densely forested environments with minimal human annotations. This alleviates the sim-to-real transfer issues prevalent in RL methods.
- A novel vegetation-aware motion planner that switches between (1). a holonomic velocity space to minimize the risk of entrapment in vegetation assessed from proprioceptive signals from the legged robot's joints, and (2). a non-holonomic velocity space to navigate narrow passages between solid, non-pliable vegetation. Further, it generates dynamically feasible, smooth candidate actions/velocities to be assessed by VAPOR's Q-network.

II. RELATED WORK

In this section, we discuss the existing literature on vegetation perception in outdoor environments. We also cover the previous offline reinforcement learning methods used for navigation. Finally, we discuss the existing holonomic planning methods.

A. Outdoor Vegetation Perception

Navigating robots in outdoor environments, particularly through vegetation, is a challenging task that has received increasing attention in recent years [4], [12], [13]. Existing approaches tackle this issue from multiple perspectives, including various sensory modalities and learning techniques. For instance, [14] adopts a semi self-supervised approach to estimate the support surface in vegetation. They employ 3D point clouds and RGB images as exteroceptive sensors. Despite their promising results, the system requires manual labeling, which could be time-consuming and less scalable for real-world deployments. In [4], the authors use RGB images and 2D Lidar to create traversability cost maps in dense vegetation environments. Another work is presented in [15], where an inferred red (IR) sensor is used along a color camera for vegetation detection. While effective in certain conditions, these vision-based methods are often vulnerable

to environmental factors such as changing light conditions and motion blur, thereby limiting their robustness.

Iberraken et al. [16] take a different approach by relying only on 2D LiDAR for navigation through vegetation, particularly vineyard fields. This method detects crop rows using wheeled robots which facilitate agriculture operations such as monitoring and cropping.

Some recent works have shifted their focus from external sensors to proprioceptive methods for perceiving vegetation [17], [18]. While proprioception offers reliable feedback about the robot's internal state, it inherently lacks the capability for look-ahead predictions before traversing a given terrain, especially in the absence of exteroceptive sensors.

Our work takes a distinct path by promoting the exclusive use of 3D LiDAR for robust and efficient navigation through outdoor vegetation. Unlike some existing methods that rely on manual labeling, our approach is fully automated, aiming to address many of the limitations observed in the existing solutions and offering a more comprehensive and scalable alternative.

B. Offline RL based Robot Navigation

Reinforcement Learning (RL) has been a foundation in the field of robotic navigation [19], [20], [21], [22], providing methods for autonomous decision-making based on interaction with the environment. However, traditional online RL often falls short in situations where real-time data collection is either impractical or the lack of realistic simulation which increases the sim-to-real gap [23] e.g., navigating through dense vegetation or hazardous or complex terrains. On the other hand, Offline RL has emerged as a promising alternative, designed to optimize policies based on pre-collected datasets. Among the foundational works in Offline RL is the study by Levine et al. [24], which outlines the key methodologies and challenges. Imitation Learning (IL) is one of the early techniques that leverages collected data [25], [26], [25]. However, IL is often restricted by the limitations of the human operator(expert) who collected the data, meaning it can't generally surpass the operator's performance. In contrast, Offline RL aims to optimize the behavioral policy based on the dataset, offering the potential for more generalized and sometimes superior strategies [27], [28], [11] Kostrikov et al. [27] introduce Implicit Q-Learning (IQL) which implicitly estimates the value function without querying the Q function of unseen actions. While IQL shows promise, it struggles in tasks with long planning horizons. Shah et al. [11] mitigate this limitation by combining IQL with topological graphs in their ReViND work. Nevertheless, their method primarily relies on RGB sensor data, which may be unreliable in outdoor settings where environmental changes could happen and negatively affect the learned policy.

On the other hand, [29] develops Conservative Q-Learning (CQL) to enhance the robustness of the learned policy. This method lower-bounds the true value of its learned Q function. Following its superior performance with complex data distribution, we extend this method by exclusively

employing 3D LiDAR point clouds for perception, offering a unique approach compared to previous methods.

Emerging work in Offline RL includes the use of model-based approaches. For example, Diehl et al. [30] incorporate uncertainty estimates into their learning algorithm, and Li et al. [28] add hierarchical goals to deal with long-term planning. While these contributions advance the general methodology of Offline RL, they don't fully focus on robotic navigation in unstructured outdoor environments.

C. Holonomic Planning

Traditional robotic planning often focuses on non-holonomic robotic planners, largely because many robots including wheeled robots, inherently possess non-holonomic constraints [31], [32], [33], [34]. Conversely, Robots with higher degrees of freedom, such as multi-legged or manipulator robots, can benefit from holonomic planning methods [35], [36]. The main advantage of using a holonomic planner is the ability to freely move in the workspace without any constraint on the velocity and orientation, which is particularly useful for complex tasks that require complicated paths or orientations.

III. BACKGROUND

A. Offline Reinforcement Learning

We mathematically formulate our navigation problem as a Markov Decision Process (MDP) with continuous states and actions. Hence, our MDP \mathcal{M} can be defined as $\mathcal{M} := \{\mathcal{S}, \mathcal{A}, \mathbb{P}, r, \gamma\}$, where \mathcal{S}, \mathcal{A} denote state and action spaces, $\mathbb{P}(s'|s, a)$ represents transition dynamics, $r(s, a)$ is the reward function, and $\gamma \in (0, 1)$ denotes the discount factor. The objective of RL is to learn a behavior policy $\pi_\theta(a|s)$ parameterized by θ that maximizes the discounted cumulative reward return.

Offline RL particularly aims to learn policies from existing data sets instead of explicitly interacting with the environment. Hence, for a given dataset $\mathcal{D} = \{(s_j, a_j, r_j, s'_j) | s_j, s'_j \in \mathcal{S}; a_j \in \mathcal{A}; j = 1, 2, \dots, N\}$, offline RL algorithms attempt to learn a policy $\pi_\theta(a|s)$ that maximizes the discounted reward return. However, leveraging the standard RL algorithms for offline RL leads to poor performance due to overfitting and distributional shifts. Especially since the offline RL algorithms learn to deviate from the behavior in the dataset and make counterfactual predictions for unseen outcomes. In particular, the existing value-based off-policy RL methods such as Q learning typically overestimate the value function predictions for unseen outcomes, which results in erroneous and overly optimistic estimations. To mitigate this issue, Conservative Q Learning (CQL)[29] regularizes the Q-values during training to learn conservative and lower-bound estimates of the value function. Hence, in this work, we incorporate Conservative Q Learning (CQL) with Soft Actor-Critic (SAC) proposed in [37] as our base offline RL algorithm.

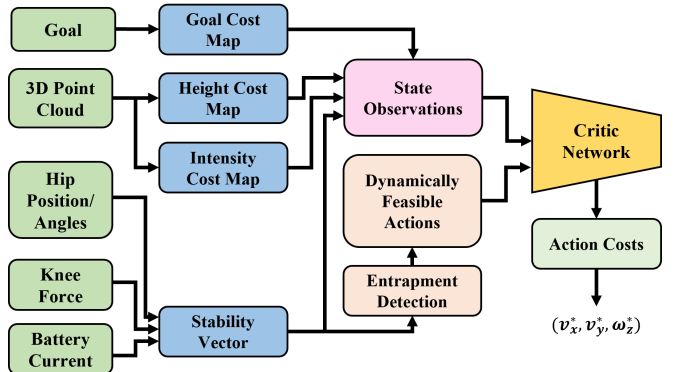


Fig. 2: System Architecture

B. Channel and Spatial Attention

Our observation inputs include three robot-centric 2D cost maps that reflect different properties such as the density and height of the surrounding objects, and distance to the goal. We concatenate these three cost maps to construct a 3D map input to the RL pipeline. Hence, robust perception requires learning both neighborhood properties within a cost map (i.e., spatial attention) and the correlation between the multiple cost maps (i.e., channel attention).

IV. VAPOR: VEGETATION-AWARE PLANNING USING OFFLINE REINFORCEMENT LEARNING

A. Dataset

Our raw data is collected by operating a Boston Dynamics Spot robot equipped with a 360° 3D Velodyne LiDAR; and the robot's inbuilt sensors measure odometry, joint data, and motor current. The data collection process is conducted by manually operating the robot in outdoor vegetation including grass, bushes, and trees with different levels of density and complexity. Hence, the raw data set does not have any goal-conditioning or goal-reaching policy.

1) *Goal-conditioned Dataset Generation*: To generate goal-conditioned data set \mathcal{D} , we consider random trajectory segments from the raw dataset, i.e., we select a random sample for the initial position and a subsequent sample in the same raw trajectory as the goal. The subsequent goal sample is selected such that it is $\sim 8 - 20$ meters away from the robot's initial position. Hence, our processed dataset $\mathcal{D} = \{(s_j, a_j, r_j, s'_j) | j = 1, 2, \dots, N\}$, where s_j, a_j, r_j, s'_j denotes the current state, current action, reward, and next state of the j^{th} data sample, respectively. We explain the details of the state observations, actions, and reward formulation in the sub-sections below.

B. State Observations from Multi-sensor Data

Our state observations $s \in \mathcal{S}$ are obtained by pre-processing the raw sensory data collected from both the exteroceptive and proprioceptive sensors of the robot. We acquire exteroceptive sensing from a 3D LiDAR, which provides a point cloud with intensity $P^{\{x, y, z, i\}}$, and the robot's odometer that provides its position w.r.t. odometry frame (x_r^O, y_r^O) and orientation of the robot (i.e., roll (ϕ_{roll}) ,

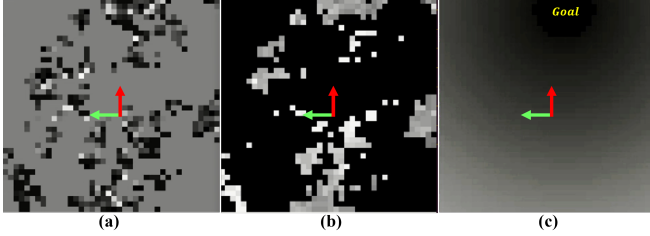


Fig. 3: Robot-centric cost map state observations from exteroceptive sensing: (a) Point cloud-based intensity cost map \mathcal{C}_i that indicates the density of the surrounding objects using LiDAR reflectance; (b) Height cost map \mathcal{C}_h that represents the maximum height of the objects derived from the point cloud; (c) Goal cost map \mathcal{C}_g that indicates the distance to the goal from the robot's neighborhood. Light colors indicate higher costs and dark areas represent lower costs.

pitch (ϕ_{pitch}), yaw (ϕ_{yaw}) angles). A given LiDAR point $p_{xyzi} = \{p_{xyzi} \in P^{\{x,y,z,i\}} | x, y, z \in \mathbb{R}; i \in [0, i_{max}]\}$, where x, y, z , represent point locations w.r.t. the sensor and i denotes the point intensity. Proprioceptive sensing is obtained from the robot's joint positions, force feedback, and the battery's current consumption.

We preprocess the aforementioned sensory data to generate two types of state observations: 1.) S_{ext} : A set of robot-centric cost maps that reflect the solidity and height of the surrounding objects, and distance to the goal using exteroceptive sensors; 2.) S_{prop} : A vector that quantifies the robot's stability using proprioception. Hence, our final state observations $s = [S_{ext}, S_{prop}] \in \mathcal{S}$.

1) *Layered Cost Map Generation from Exteroception Data* : Robot navigation in outdoor vegetation requires identifying the navigable regions from solid and dense vegetation such as trees, bushes, etc. Specifically, the height and solidity of the vegetation in the robot's vicinity are two important properties that need to be identified during perception. Moreover, spatial information of the goal location is necessary to perform successful goal-reaching tasks. Hence, we propose three robot-centric 2D cost maps, Intensity cost map (\mathcal{C}_i), Height cost map (\mathcal{C}_h), and Goal cost map (\mathcal{C}_g), to represent the solidity and height of the surrounding objects/vegetation, and distance to the goal respectively.

All three cost maps $\mathcal{C}_i, \mathcal{C}_h$ and, \mathcal{C}_g are $n \times n$ matrices with the robot positioned at the center as depicted in Fig. 3. Each element $\mathcal{C}(l, m) \in [0, 100] \quad \forall l, m = 0, 1, \dots, n - 1$ of a cost map represents a grid d_{lm}^{grid} in the real world of size $\beta_{res} \times \beta_{res}$ square meters with β_{res} denoting the map resolution.

Intensity Cost Map (\mathcal{C}_i): We employ LiDAR intensity values, a method previously used in various robotics applications [38], [39], [40], to construct an Intensity Cost Map \mathcal{C}_i . Here, we demonstrate that 3D LiDAR intensity can be used to identify the solidity of different types of vegetation. This is especially true since the LiDAR reflectance power (i.e., intensity) is directly proportional to the solidity of the corresponding objects. Hence, we observe that grass, bushes, and trees result in distinct LiDAR intensity values based on

the level of vegetation density. (i.e., higher intensity denotes solid objects and vice versa). We calculate elements of \mathcal{C}_i as,

$$\mathcal{C}_i(l, m) = \frac{\sum_x \sum_y i}{\beta_{res}^2} \quad \forall x, y \in d_{lm}^{grid}. \quad (1)$$

Height Cost Map (\mathcal{C}_h): We generate \mathcal{C}_h to represent the maximum heights of the objects in each grid location d_{lm}^{grid} . To this end, element (l, m) of \mathcal{C}_h is obtained by,

$$\mathcal{C}_h(l, m) = \max(z) \quad \forall x, y \in d_{lm}^{grid}, \quad (2)$$

where higher values in $\mathcal{C}_h(l, m)$ indicate taller objects.

Goal Cost Map (\mathcal{C}_g): The goal cost map is designed to represent the distance to the goal from each grid location d_{lm}^{grid} . Since we assume a robot-centric cost map, the real-world position of each grid d_{lm}^{grid} can be calculated w.r.t. the robot as,

$$\begin{bmatrix} x_{grid}^R \\ y_{grid}^R \end{bmatrix} = \begin{bmatrix} l - \frac{n}{2} \\ m - \frac{n}{2} \end{bmatrix} \beta_{res}, \quad (3)$$

where $n \times n$ is the size of the cost map with the robot located at $(\frac{n}{2}, \frac{n}{2})$. To obtain the position of the grid w.r.t. the odometry frame, we can use the transformation matrix between the robot frame and the odometry frame as below.

$$\begin{bmatrix} x_g^O \\ y_g^O \end{bmatrix} = \begin{bmatrix} x_r^O \\ y_r^O \end{bmatrix} + \begin{bmatrix} \cos(\phi_{yaw}) & -\sin(\phi_{yaw}) \\ \sin(\phi_{yaw}) & \cos(\phi_{yaw}) \end{bmatrix} \begin{bmatrix} x_{grid}^R \\ y_{grid}^R \end{bmatrix} \quad (4)$$

Let x_g^O, y_g^O be the goal position w.r.t. the odometry frame. Then, we calculate the element (l, m) of \mathcal{C}_g as,

$$\mathcal{C}_g(l, m) = \frac{\alpha_g \cdot \left(\sqrt{(x_g^O - x_{grid}^O)^2 + (y_g^O - y_{grid}^O)^2} \right)}{d_{tot}}, \quad (5)$$

where d_{tot} is the total distance to the goal from the robot's starting position and $\alpha_g \in \mathbb{R}$ is a tunable parameter.

Finally, we obtain our state observation from the exteroception S_{ext} by concatenating the derived cost maps. Hence, $S_{ext} = \{\mathcal{C}_i, \mathcal{C}_h, \mathcal{C}_g\}$ of shape $n \times n \times 3$.

2) *Stability Observation from Proprioception:* We utilize proprioception to quantify the robot's stability. Specifically, we incorporate data acquired from the robot's joint positions, forces, and battery current for proprioceptive sensing. To this end, we denote the raw proprioceptive signals as $H_{prop} = [h_1^{x/y}, h_2^{x/y}, h_3^{x/y}, h_4^{x/y}, f_1, f_2, f_3, f_4, I_b]$, where, $h_k^{x/y}, k = 1, \dots, 4$ are the hip positions along x/y axis, $f_k, k = 1, \dots, 4$ are the knee forces and I_b is battery's current consumption.

Then, based on [17], the raw proprioception vector H_{prop} is prepossessed into a refined vector M_{prop} , defined as:

$$M_{prop} = [\alpha^1, \alpha^2, \alpha^3, \alpha^4, \alpha^5, \alpha^6, \alpha^7, \alpha^8, I_b] \quad (6)$$

Here, α^{1-8} are the outputs of preprocessing step applied to H_{prop} and I_b is the battery current. For further details of the preprocessing steps, we refer to [17]. Subsequently, we use the principal components analysis (PCA) to extract stability variances (σ_{PC1}^2 and σ_{PC2}^2), which serve as additional observations for our method. Hence, we define our

resulting proprioceptive state observation vector as: $S_{prop} = [\sigma_{PC1}^2, \sigma_{PC2}^2], \sigma_{PC1}^2 > 0, \sigma_{PC2}^2 > 0$.

These variances reflect the stability of the robot, with stable terrains like asphalt leading to lower variances, and unstable terrain leading to higher values.

Lastly, We derive our final state observation as $s = [S_{ext}, S_{prop}]$ by combining both exteroceptive and proprioceptive state observations.

C. Offline Reinforcement Learning Using CQL-SAC

We train an offline RL navigation policy using the CQL-SAC [29] algorithm and our dataset \mathcal{D} . The standard SAC algorithm uses maximum entropy regularization to find the optimal policy that maximizes both the expected long-term reward and entropy. In CQL-SAC [29], an additional CQL regularizer is introduced to train the Q-value function in the standard SAC.

Our CQL-SAC implementation incorporates two critic networks and an actor-network. The policy actor-network (i.e., $\pi_\theta(a|s)$) estimates the parameters θ of the policy distribution, which provides the conditional probability of taking action a given the state observation s . In our context, this policy distribution is Gaussian parameterized by the mean μ_θ and standard deviation σ_θ . Further, the two critic networks are Q networks (i.e., $Q_1(s, a; \pi_\theta), Q_2(s, a; \pi_\theta)$) that take state observation s and action a as inputs to estimate the expectation of the value function. We design the actor and critic networks as follows.

1) Actor and Critic Networks: Our actor and critic network architecture with layer dimensions is presented in Fig. 4 with layer dimensions. In both networks, we use two separate network branches to process the exteroceptive S_{ext} and proprioceptive S_{prop} observations in our input state s . The first branch uses four convolution layers with the first two layers followed by spatial and channel attention modules to process the layered costmap input provided by S_{ext} . We use spatial attention to encode spatial neighborhood properties in individual cost maps and channel attention to encode the feature association between the cost maps. The second branch uses three linear layers to process the 1D state inputs in S_{prop} . We concatenate the outputs from the two branches into a linear layer and pass another two linear layers through to obtain the outputs.

Since the critic networks take both the action and state inputs, we use an additional branch to process the action by passing two linear layers through before concatenating with the state observation branches. All the hidden layers in the network are followed by *ReLU* activation.

2) Reward Functions: The reward function r_{tot} is formulated to obtain robot actions that lead to desired navigation behavior. In this work, we are primarily interested in three navigation behaviors: 1) Goal reaching; 2) Avoiding dense/solid objects while navigating through pliable vegetation; and 3) Minimizing the overall energy consumption. We introduce three reward terms r_{goal}, r_{veg} , and r_{energy} to achieve the aforementioned behaviors. Hence, the total

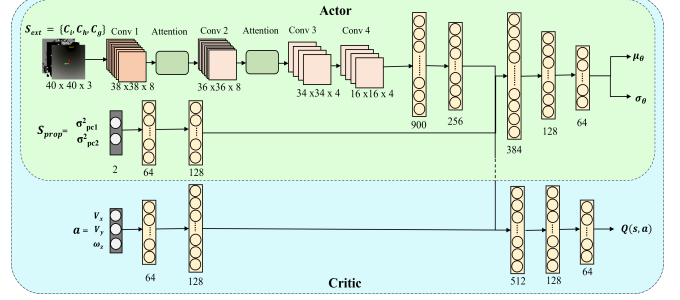


Fig. 4: Model Architecture

reward obtained by the robot for a given sample is calculated as,

$$r_{tot} = \beta_1 r_{goal} + \beta_2 r_{veg} + \beta_3 r_{energy}, \quad (7)$$

where $\beta_j \in \mathbb{R} \forall j = 1, 2, 3$ are tunable parameters to weigh the reward terms. We design r_{goal} based on the robot's current distance d_g to the goal to encourage moving towards the goal. Hence,

$$r_{goal} = \frac{\lambda_{g1} d_{tot}}{d_g} \mathbb{1}_{\{d_g > d_{th}\}} + \lambda_{g2} \mathbb{1}_{\{d_g \leq d_{th}\}}, \quad (8)$$

where $\lambda_{g1}, \lambda_{g2} \in \mathbb{R}$ are adjustable parameters and d_{th} is the goal reaching threshold.

The vegetation reward r_{veg} is a penalty that indicates the density of the nearby vegetation (i.e, higher the density lower the reward). To this end, we consider three neighborhood areas with radii 0.5, 1.5 and 2.5 meters that are from the robot. Let, A_1, A_2 and A_3 denote the sets that contain corresponding elements in the intensity cost map \mathcal{C}_i . Then, r_{veg} is calculated as,

$$r_{veg} = - \sum_{k=1,2,3} \left(\frac{\lambda_{v1}}{|A_k|} \sum_{l,m \in A_k} \mathcal{C}_i(l, m) \right), \quad (9)$$

where the tunable parameters are set such that $\lambda_{v1} > \lambda_{v2} > \lambda_{v3} \in \mathbb{R}$ to ensure higher penalties for the dense vegetation in the robot's nearby vicinity. $|A_k|$ denotes cardinality of the set A_k .

We incorporate r_{energy} to penalize high energy consumption during navigation. Since the overall energy consumption of the robot is directly proportional to the current I_b drawing from the robot's battery, we calculate r_{energy} as,

$$r_{energy} = -\lambda_e I_b, \quad (10)$$

where $\lambda_e \in \mathbb{R}^+$ is a weight parameter.

3) Critic Networks for State-action Evaluation: Even though we train an end-to-end navigation policy using CQL-SAC on our data set \mathcal{D} , we do not use the actions output by the trained policy $\pi_\theta(a|s)$ in Actor network for navigation. Instead, we leverage a trained Critic Network to evaluate the quality of the set of actions (using the $Q(s, a)$ values from the Critic networks) generated by a holonomic planner. Intuitively, Q values for a given state-action pair indicate how

well the action obtains desirable behaviors imposed by the reward function. Since CQL-SAC includes two Q networks as critics (i.e., $Q_1(s, a; \pi_\theta)$ and $Q_2(s, a; \pi_\theta)$) we choose the Q network with the lowest training loss. We refer to this selected Critic network as $Q_{min}(s, a; \pi_\theta)$ from here on.

D. Adaptive Holonomic Planning

To generate dynamically feasible candidate actions to be evaluated using the Q-functions $Q_{min}(s, a; \pi_\theta)$, we formulate a novel adaptive holonomic planner. An action $a \in \mathcal{A}$ for our robot can be denoted as $a = (v_x, v_y, \omega_z)$. The planner uses a 3-dimensional velocity space ($V_s \subset \mathcal{A}$) defined as $V_s = \{(v_x, v_y, \omega_z) | -v_{max} \leq v_x, v_y \leq v_{max}, -\omega_{max} \leq \omega_z \leq \omega_{max}\}$. Here, v_x and v_y denote the linear velocities along the x and y directions respectively, and ω_z represents the angular velocity about the vertical z-axis. v_{max} and ω_{max} are the maximum linear and angular velocity limits. Additionally, the planner uses the set of reachable/dynamically feasible velocities from the current velocities within an interval Δt based on acceleration limits as $V_r = \{[v_x - \dot{v}_{max}\Delta t, v_x + \dot{v}_{max}\Delta t], [v_y - \dot{v}_{max}\Delta t, v_y + \dot{v}_{max}\Delta t], [\omega_z - \dot{\omega}_{max}\Delta t, \omega_z + \dot{\omega}_{max}\Delta t]\}$. Here, \dot{v}_{max} , and $\dot{\omega}_{max}$ are the robot's maximum linear and angular acceleration limits.

While navigating through dense vegetation consisting of vines, tall grass, and bushes, the legged robot faces a high risk of entrapment since the vegetation could intertwine with the robot's legs, restricting its motion. This is exacerbated when the robot performs angular motions because it aids the vegetation in helically twirling on its legs (intuitively similar to rotating a fork on spaghetti). Therefore, in such scenarios, the robot's angular motion must be restricted. On the other hand, in scenarios with narrow passages, the rectangularly shaped robot must be capable of performing angular motions to traverse through. Such behaviors are also desirable when the robot is equipped with a sensor with a limited FOV that needs to be pointed in a specific direction. To accommodate both scenarios, we restrict V_s based on the following condition:

$$\text{Cond : } \sqrt{\sigma_1^2 + \sigma_2^2} > \Gamma \text{ and } \mathcal{C}_i(l, m) \in [50, 75] \quad (11)$$

$$\forall l, m \in A_2.$$

$$V_s = \begin{cases} \{(v_x, v_y, 0)\}, & \text{if Cond is True,} \\ \{(v_x, 0, \omega_z)\}, & \text{Otherwise,} \end{cases} \quad (12)$$

where $v_x, v_y \in [-v_{max}, v_{max}]$, and $\omega_z \in [-\omega_{max}, \omega_{max}]$. The corresponding V_r is calculated from the restricted V_s by omitting either v_y or ω_z based on the environment. The best action a^* for the robot to execute given the current state s can then be found as,

$$a^* = \underset{a_k \in V_r}{\text{argmax}}(Q_{min}(s, a_k)). \quad (13)$$

V. RESULTS AND ANALYSIS

A. Implementation

Our Offline RL policy is implemented using PyTorch and our model is trained on a workstation with an Intel Xeon 3.6 GHz processor and an Nvidia Titan GPU. For real-time deployment and inference, we use the Spot robot from Boston Dynamics equipped with a VLP16 Velodyne LiDAR, an onboard Intel NUC 11, which includes an Intel i7 CPU and an NVIDIA RTX 2060 GPU.

B. Evaluation Metrics

We incorporate the following metrics to compare our method's navigation performance with three recent offline RL algorithms: CQL-SAC (end-to-end)[29]; IQL [27]; BCO [41] and two outdoor navigation algorithms: VERN [4]; and DWA [9]. We further perform two ablation studies: VAPOR w/o Proprioception; and VAPOR w/o Attention to highlight the benefits of our approach.

CQL-SAC [29] is the end-to-end navigation policy $\pi_\theta(a|s)$ obtained by the fully trained actor network of our implementation. IQL [27] is an offline RL algorithm that approximates the policy improvements implicitly by considering the state value function as a random variable, with randomness determined by the action. BCO [41] (Behavioral Cloning from Observations) is an autonomous imitation learning approach that uses state-action pairs from expert demonstrations to learn a policy. We train all the aforementioned offline RL methods on our data set \mathcal{D} for fair comparison.

Success Rate - The number of times the robot reached its goal while avoiding collisions with *solid and dense vegetation* over the total number of attempts.

Avg. Current Consumption - The average battery current consumption during a navigation task (i.e., $\sum_{traj} I_b$).

Normalized Traj. Length - The robot's trajectory length normalized using the straight-line distance to the goal for both successful and unsuccessful trajectories.

Expected Cumulative Reward - Average cumulative reward return of a policy during a navigation task.

C. Testing Scenarios

We compare our method's navigation performance in the real-world outdoor scenarios below.

- **Scenario 1** - Contains narrow passages between shrubs, and trees in a mulch surface.
- **Scenario 2** - Dense bushes that lead to entrapment, sparse grass, and trees.
- **Scenario 3** - Thin grass, shrubs, and trees with narrow openings under low light conditions.
- **Scenario 4** - Dense grass, fallen branches, vines, and trees.

VI. CONCLUSIONS, LIMITATIONS AND FUTURE WORK

REFERENCES

- [1] N. S. Naik, V. V. Shete, and S. R. Danve, "Precision agriculture robot for seeding function," in 2016 international conference on inventive computation technologies (ICICT), vol. 2. IEEE, 2016, pp. 1–3.



Fig. 5: Example navigation scenarios where the robot requires to navigate through dense vegetation and tall grass under different lighting conditions.

[2] S. Karma, E. Zorba, G. Pallis, G. Statheropoulos, I. Balta, K. Mikedi, J. Vamvakari, A. Pappa, M. Chalaris, G. Xanthopoulos, *et al.*, “Use of unmanned vehicles in search and rescue operations in forest fires: Advantages and limitations observed in a field trial,” *International journal of disaster risk reduction*, vol. 13, pp. 307–312, 2015.

[3] S. Li, C. Feng, Y. Niu, L. Shi, Z. Wu, and H. Song, “A fire reconnaissance robot based on slam position, thermal imaging technologies, and ar display,” *Sensors*, vol. 19, no. 22, p. 5036, 2019.

[4] A. J. Sathyamoorthy, K. Weerakoon, T. Guan, M. Russell, D. Conover, J. Pusey, and D. Manocha, “Vern: Vegetation-aware robot navigation in dense unstructured outdoor environments,” *arXiv preprint arXiv:2303.14502*, 2023.

[5] G. Kahn, P. Abbeel, and S. Levine, “Badgr: An autonomous self-supervised learning-based navigation system,” *IEEE Robotics and Automation Letters*, vol. 6, no. 2, pp. 1312–1319, 2021.

[6] K. Weerakoon, A. J. Sathyamoorthy, J. Liang, T. Guan, U. Patel, and D. Manocha, “Graspe: Graph based multimodal fusion for robot navigation in unstructured outdoor environments,” *arXiv preprint arXiv:2209.05722*, 2022.

[7] A. N. Catapang and M. Ramos, “Obstacle detection using a 2d lidar system for an autonomous vehicle,” in *2016 6th IEEE International Conference on Control System, Computing and Engineering (ICCSCE)*. IEEE, 2016, pp. 441–445.

[8] M. Bijelic, T. Gruber, F. Mannan, F. Kraus, W. Ritter, K. Dietmayer, and F. Heide, “Seeing through fog without seeing fog: Deep multimodal sensor fusion in unseen adverse weather,” in *Proceedings of the IEEE/CVF Conference on Computer Vision and Pattern Recognition*, 2020, pp. 11 682–11 692.

[9] D. Fox, W. Burgard, and S. Thrun, “The dynamic window approach to collision avoidance,” *IEEE Robotics & Automation Magazine*, vol. 4, no. 1, pp. 23–33, 1997.

[10] J. Liang, U. Patel, A. J. Sathyamoorthy, and D. Manocha, “Crowdsteer: Realtime smooth and collision-free robot navigation in densely crowded scenarios trained using high-fidelity simulation,” in *Proceedings of the Twenty-Ninth International Conference on International Joint Conferences on Artificial Intelligence*, 2021, pp. 4221–4228.

[11] D. Shah, A. Bhorkar, H. Leen, I. Kostrikov, N. Rhinehart, and S. Levine, “Offline reinforcement learning for visual navigation,” *arXiv preprint arXiv:2212.08244*, 2022.

[12] J. Iqbal, R. Xu, S. Sun, and C. Li, “Simulation of an autonomous mobile robot for lidar-based in-field phenotyping and navigation,” *Robotics*, vol. 9, no. 2, p. 46, 2020.

[13] G. Kahn, P. Abbeel, and S. Levine, “Badgr: An autonomous self-supervised learning-based navigation system,” *IEEE Robotics and Automation Letters*, vol. 6, no. 2, pp. 1312–1319, 2021.

[14] A. Li, C. Yang, J. Frey, J. Lee, C. Cadena, and M. Hutter, “Seeing through the grass: Semantic pointcloud filter for support surface learning,” *arXiv preprint arXiv:2305.07995*, 2023.

[15] D. L. Stone, G. Shah, Y. Motai, and A. J. Aved, “Vegetation segmentation for sensor fusion of omnidirectional far-infrared and visual stream,” *IEEE Journal of Selected Topics in Applied Earth Observations and Remote Sensing*, vol. 12, no. 2, pp. 614–626, 2019.

[16] D. Iberraken, F. Gaurier, J.-C. Roux, C. Chaballier, and R. Lenain, “Autonomous vineyard tracking using a four-wheel-steering mobile robot and a 2d lidar,” *AgriEngineering*, vol. 4, no. 4, pp. 826–846, 2022.

[17] M. Elnoor, A. J. Sathyamoorthy, K. Weerakoon, and D. Manocha, “Pronav: Proprioceptive traversability estimation for legged robot navigation in outdoor environments,” 2023.

[18] Z. Jian, Z. Liu, H. Shao, X. Wang, X. Chen, and B. Liang, “Path generation for wheeled robots autonomous navigation on vegetated terrain,” *arXiv preprint arXiv:2306.08977*, 2023.

[19] A. Faust, K. Oslund, O. Ramirez, A. Francis, L. Tapia, M. Fiser, and J. Davidson, “Prm-rl: Long-range robotic navigation tasks by combining reinforcement learning and sampling-based planning,” in *2018 IEEE international conference on robotics and automation (ICRA)*. IEEE, 2018, pp. 5113–5120.

[20] D. Dugas, J. Nieto, R. Siegwart, and J. J. Chung, “Navrep: Unsupervised representations for reinforcement learning of robot navigation in dynamic human environments,” in *2021 IEEE International Conference on Robotics and Automation (ICRA)*. IEEE, 2021, pp. 7829–7835.

[21] U. Patel, N. K. S. Kumar, A. J. Sathyamoorthy, and D. Manocha, “Dwa-rl: Dynamically feasible deep reinforcement learning policy for robot navigation among mobile obstacles,” in *2021 IEEE International Conference on Robotics and Automation (ICRA)*. IEEE, 2021, pp. 6057–6063.

[22] K. Weerakoon, A. J. Sathyamoorthy, U. Patel, and D. Manocha, “Terp: Reliable planning in uneven outdoor environments using deep reinforcement learning,” in *2022 International Conference on Robotics and Automation (ICRA)*. IEEE, 2022, pp. 9447–9453.

[23] T. Zhang and H. Mo, “Reinforcement learning for robot research: A comprehensive review and open issues,” *International Journal of Advanced Robotic Systems*, vol. 18, no. 3, p. 17298814211007305, 2021.

[24] S. Levine, A. Kumar, G. Tucker, and J. Fu, “Offline reinforcement learning: Tutorial, review, and perspectives on open problems,” *arXiv preprint arXiv:2005.01643*, 2020.

[25] F. Codevilla, M. Müller, A. López, V. Koltun, and A. Dosovitskiy, “End-to-end driving via conditional imitation learning,” in *2018 IEEE international conference on robotics and automation (ICRA)*. IEEE, 2018, pp. 4693–4700.

[26] D. Silver, J. A. Bagnell, and A. Stentz, “Applied imitation learning for autonomous navigation in complex natural terrain,” in *Field and Service Robotics: Results of the 7th International Conference*. Springer, 2010, pp. 249–259.

[27] I. Kostrikov, A. Nair, and S. Levine, “Offline reinforcement learning with implicit q-learning,” *arXiv preprint arXiv:2110.06169*, 2021.

[28] J. Li, C. Tang, M. Tomizuka, and W. Zhan, “Hierarchical planning through goal-conditioned offline reinforcement learning,” *IEEE Robotics and Automation Letters*, vol. 7, no. 4, pp. 10 216–10 223, 2022.

[29] A. Kumar, A. Zhou, G. Tucker, and S. Levine, “Conservative q-learning for offline reinforcement learning,” *Advances in Neural Information Processing Systems*, vol. 33, pp. 1179–1191, 2020.

[30] C. Diehl, T. S. Sieverich, M. Krüger, F. Hoffmann, and T. Bertram, “Uncertainty-aware model-based offline reinforcement learning for automated driving,” *IEEE Robotics and Automation Letters*, vol. 8, no. 2, pp. 1167–1174, 2023.

[31] K. Yang, S. Moon, S. Yoo, J. Kang, N. L. Doh, H. B. Kim, and S. Joo, “Spline-based rrt path planner for non-holonomic robots,” *Journal of Intelligent & Robotic Systems*, vol. 73, no. 1–4, pp. 763–782, 2014.

[32] A. Khan, I. Noreen, and Z. Habib, “On complete coverage path

planning algorithms for non-holonomic mobile robots: Survey and challenges.” *J. Inf. Sci. Eng.*, vol. 33, no. 1, pp. 101–121, 2017.

[33] H.-W. Chae, J.-H. Choi, and J.-B. Song, “Robust and autonomous stereo visual-inertial navigation for non-holonomic mobile robots,” *IEEE Transactions on Vehicular Technology*, vol. 69, no. 9, pp. 9613–9623, 2020.

[34] S. Eshtehardian and S. Khodaygan, “A continuous rrt*-based path planning method for non-holonomic mobile robots using b-spline curves,” *Journal of Ambient Intelligence and Humanized Computing*, vol. 14, no. 7, pp. 8693–8702, 2023.

[35] R. Holmberg and O. Khatib, “Development and control of a holonomic mobile robot for mobile manipulation tasks,” *The International Journal of Robotics Research*, vol. 19, no. 11, pp. 1066–1074, 2000.

[36] M. Alireza, D. Vincent, and W. Tony, “Experimental study of path planning problem using emcoa for a holonomic mobile robot,” *Journal of Systems Engineering and Electronics*, vol. 32, no. 6, pp. 1450–1462, 2021.

[37] T. Haarnoja, A. Zhou, P. Abbeel, and S. Levine, “Soft actor-critic: Off-policy maximum entropy deep reinforcement learning with a stochastic actor,” in *International conference on machine learning*. PMLR, 2018, pp. 1861–1870.

[38] L. Di Giammarino, I. Aloise, C. Stachniss, and G. Grisetti, “Visual place recognition using lidar intensity information,” in *2021 IEEE/RSJ International Conference on Intelligent Robots and Systems (IROS)*. IEEE, 2021, pp. 4382–4389.

[39] T. D. Barfoot, C. McManus, S. Anderson, H. Dong, E. Beerepoot, C. H. Tong, P. Furgale, J. D. Gammell, and J. Enright, “Into darkness: Visual navigation based on a lidar-intensity-image pipeline,” in *Robotics Research: The 16th International Symposium ISRR*. Springer, 2016, pp. 487–504.

[40] L. Weerakoon, G. S. Herr, J. Blunt, M. Yu, and N. Chopra, “Cartographer glass: 2d graph slam framework using lidar for glass environments.” 2022.

[41] F. Torabi, G. Warnell, and P. Stone, “Behavioral cloning from observation,” *arXiv preprint arXiv:1805.01954*, 2018.